Evaluation of the growth behaviour of gold film surfaces evaporation-deposited on mica under different conditions

1997 J. Phys.: Condens. Matter 9 59

(http://iopscience.iop.org/0953-8984/9/1/009)

J. Phys.: Condens. Matter **9** (1997) 59–71. Printed in the UK PII: S0953-8984(97)75789-8

Evaluation of the growth behaviour of gold film surfaces evaporation-deposited on mica under different conditions

Zhi Hui Liu†, Norman M D Brown and Archibald McKinley

Surface Science Laboratory, School of Applied Biological and Chemical Sciences, University of Ulster, Coleraine, County Londonderry BT52 1SA, Northern Ireland, UK

Received 26 June 1996, in final form 9 September 1996

Abstract. A systematic AFM study of gold films deposited on mica substrates under a range of selected conditions reveals the evolution of the surface morphology of the films as a function of growth temperature, film thickness, and deposition rate. Scaling analysis shows that the growth behaviour of the surfaces of these films can be considered as self-affine fractals. The observed topography follows island-type (3D) growth processes in the majority of cases with a roughness exponent, α, in the range 0.24–0.75, or quasi-2D island growth in the remainder with $\alpha = 1.19$ or 1.45. In the latter cases, however, the two gold films grown under the particular conditions used reflect typical growth models expressing a high roughness exponent, well consistent with theoretical prediction.

1. Introduction

Study of the growth of vapour-deposited gold films, using both STM and AFM, has received significant attention in recent years [1–7]. The morphological development of such films often involves the growth of rough surfaces (or interfaces) which have been described either as self- similar [8] or as self-affine fractals [9]. It is now believed [9, 10] that rough surfaces growing under non-equilibrium conditions will have self-affine fractal forms, the surface roughness of which can be described by the so-called 'correlation function', i.e. the scale-dependent surface roughness, $W(h, L)$, which is defined as the fluctuation of the height, h, over a length scale, L. For a self-affine surface, $W(h, L)$ scales with the linear size, L, of the surface by a non-integer exponent α, called the roughness exponent, so that $W(h, L) \sim L^{\alpha}$. In complement to this, growth models such as the ballistic models [9] have been used preferentially for describing the evolution and the properties of such vapour-deposited metal films [11, 12].

Quite recently, attempts to characterize vapour-deposited gold surfaces as fractals from STM image analysis have been reported [13–15] in that the microscopic fractal character of the vapour-deposited gold film surfaces can provide additional fundamental understanding of the mechanisms responsible for the growth of such films prepared under different conditions. Work, prompted by the advent of scanning probe microscopic techniques which offer much for fractal characterization in that highly resolved 3D topographic data, ranging over extended lateral scales of micrometric to nanometric lengths, amenable to mathematical analysis, is provided. For example, methods based on Fourier analysis [16], variation [17],

† E-mail address: S057F@sperrin.ulst.ac.uk

0953-8984/97/010059+13$19.50

and island analysis [18] have been applied to STM topographic data for the study of self-affine surfaces generated by different processes. A procedure for determining the value of α from either a single STM image [15, 19] or a series of STM images scanned in differently scaled regions [20] has been described in detail. In the former case, surface profiles recorded in the scan direction are Fourier analysed and the coefficients for the individual profiles are then averaged. In the latter case, as is used in the present study, multiple images of varying scan size, L, are recorded and analysed rather than considering a single image only.

Generally, the properties of the gold films deposited depend strongly on the deposition parameters, i.e. growth temperature, film thickness, deposition rate, etc. It is expected that the gold films prepared under different conditions can develop surfaces with scaling symmetries different in detail. The SPM results reported so far have only considered gold films deposited under non-equilibrium conditions either at or near room temperatures (e.g. see [21–23]). In contrast, we report a systematic study of the scaling properties of gold film surfaces vapour-deposited on mica substrates under a variety of deposition conditions. As is expected, the prepared surfaces in all cases can be described as self-affine fractals. However, the actual value of the roughness exponent of the surfaces, as developed, changes in detail with the deposition parameters used, i.e. deposition temperature, deposition rate, and film thickness.

2. Experimental details

Deposition of gold layers on the mica substrates used was carried out in an Edwards-E12E evaporator, fitted with a substrate heater (incorporating a sensing thermocouple located behind and in contact with the substrate) mounted on a copper block, a thermo-controller, a four-windowed substrate mask, and a quartz crystal oscillator-based Intellemetrics (Model IL001) monitor for deposition rate and film thickness measurements. The mica sheets (Electron Microscopy Sciences, Washington, PA) used were cleaved in air, and promptly set on the sample stage in the evaporator vacuum chamber. The gold films used were prepared in the following way. Gold wire (diameter, 0.5 mm; purity, 99.99%; Advent Research Materials), cut to suit, was placed in a resistively heated tungsten boat in the evaporator. When the vacuum was better than 1×10^{-6} Torr, the gold was carefully melted and outgassed for $\sim$5 min. The mica substrates were then baked at a selected temperature (150, 300, or 440 °C, during each run) for more than 12 h before the gold evaporations were started. The selected substrate temperatures were maintained during gold deposition at each of the selected deposition rates and film thicknesses specified, a $\sim$1 h annealing followed thereafter. For comparison, deposition of gold films was also conducted at room temperature (RT) without prior substrate baking. The gold-coated substrates were then cooled radiatively while in vacuum to room temperature and removed from the chamber just before AFM imaging in the air. For convenience, samples either with different thicknesses or deposited at different rates were prepared in one operation by opening, for a given time in sequence, the purpose-built four-windowed substrate mask, with the substrate held at a chosen temperature at a selected deposition rate. In this way, the three groups of the samples used in the study were prepared under the conditions as designated: sample set A (deposition temperature, T = RT, 150, 300, 440 °C; film thickness, H = 1200 Å; deposition rate, $R = \sim$1.0 Å s^{-1}); sample set B (T = 300 °C; H = 100, 400, 1200 Å; $R = \sim$1.0 Å s^{-1}); and sample set C (T = 440 °C; H = 400 Å; $R = \sim$0.26, 0.78, 2.3, 6.0 Å s^{-1}). It should be noted, on the one hand, recognizing the basic operational principles of the thickness monitor, that the thicknesses of the films, as identified in the text are nominal (or averaged) values. There will be a difference between these nominal thickness data and the effective surface loading,

particularly for films formed where the metal coverage of the substrate surface is less than unity. On the other hand, the deposition temperatures of substrate referred to in the text are readings of the thermocouple before the gold deposition is commenced. In practice, however, it was found that when the substrate was held at room temperature the extended deposition times had raised the substrate temperature to some 15 °C above the ambient due to the radiative heating from the evaporation source. Such a temperature rise during deposition is determined mainly by a balance between this source of heat and the radiation losses from the specimen surfaces. It is expected, our experience apart, that this effect will be reduced significantly when the substrate is held at an elevated temperature (e.g. 300 or 440 °C) because there is a strong inverse dependence of the temperature rise (ΔT) on the substrate temperature (T_0) as $\Delta T \propto T_0^{-3}$ [24]. In this regard, the contribution of radiative heating of the evaporation source to the thermocouple reading during deposition can be eliminated, at least when the substrate is held at higher temperature.

The surface topography of the gold films prepared was investigated using an AFM system (ECS, Cambridge and Burleigh Instruments), operated in the ambient atmosphere. The integral Si_3N_4 tips and V-shaped cantilevers used for the AFM measurements have a spring constant of ∼0.1 N m^{-1} (Park Scientific Instruments, Sunnyvale, CA) and the contact force, used for imaging, between tip and surface was typically ∼1.5 nN. The AFM topographic images presented here were acquired in the constant-force mode.

The scaling analysis using the AFM data were carried out based on the 'multiple-image' method reported elsewhere [20]. Accordingly, a variety of scans, each with size L, were recorded at random locations on the gold film surfaces as prepared. The values of the RMS (root-mean-square) roughness, $W_h(L) = \langle[h(x, y) - h']^2\rangle^{1/2}$ with h' the average height, given by the instrument for the individual scans were then averaged. This procedure was repeated for numerous different scan sizes (various values of L), generating a set of average $W_h(L)$ data associated with the selected L values. All values of the RMS roughness were computed after the image was processed by standard software plane fitting procedures so as to correct for the fact that virtually all samples are macroscopically tilted with respect to the selected scan directions of the microscope used. It should be noted that plane fitting removes not only the slope due to any macroscopic tilting, but also those components of the intrinsic surface roughness of the specimen where the characteristic wavelengths significantly exceed the scan size [20]. Moreover, the finite size of the AFM tip to some extent can influence the $W_h(L)$ values measured. However, to obviate such possible effects a number of tips were used in the course of the work described. Any image artifacts attributed to tip geometry were thus eliminated. In practice, it is worth noting, our own experience apart, that it has been shown elsewhere [20, 21] that none of these factors can mask the scaling properties of the surface investigated. Therefore, the slope of a log–log plot of $W_h(L)$ against L, obtained from the AFM data, can give a value of α for a self-affine surface ($W_h(L) \sim L^{\alpha}$) within a scale range defined by a low inner cut-off lateral length, L_1, and the lateral correlation length, L_0. Correlations in the deviation of the surface height, $h(x, y)$, from the average height, h', persist over this scale range and retain the value of W_0 which characterizes the amplitude of the surface roughness or the 'thickness' of the surface.

3. Results and discussion

3.1. AFM topography

Figure 1 shows the four AFM topographic images obtained from gold films prepared under the conditions of set A (T = RT, 150, 300, 440 °C; H = 1200 Å; R = ∼1.0 Å s^{-1}).

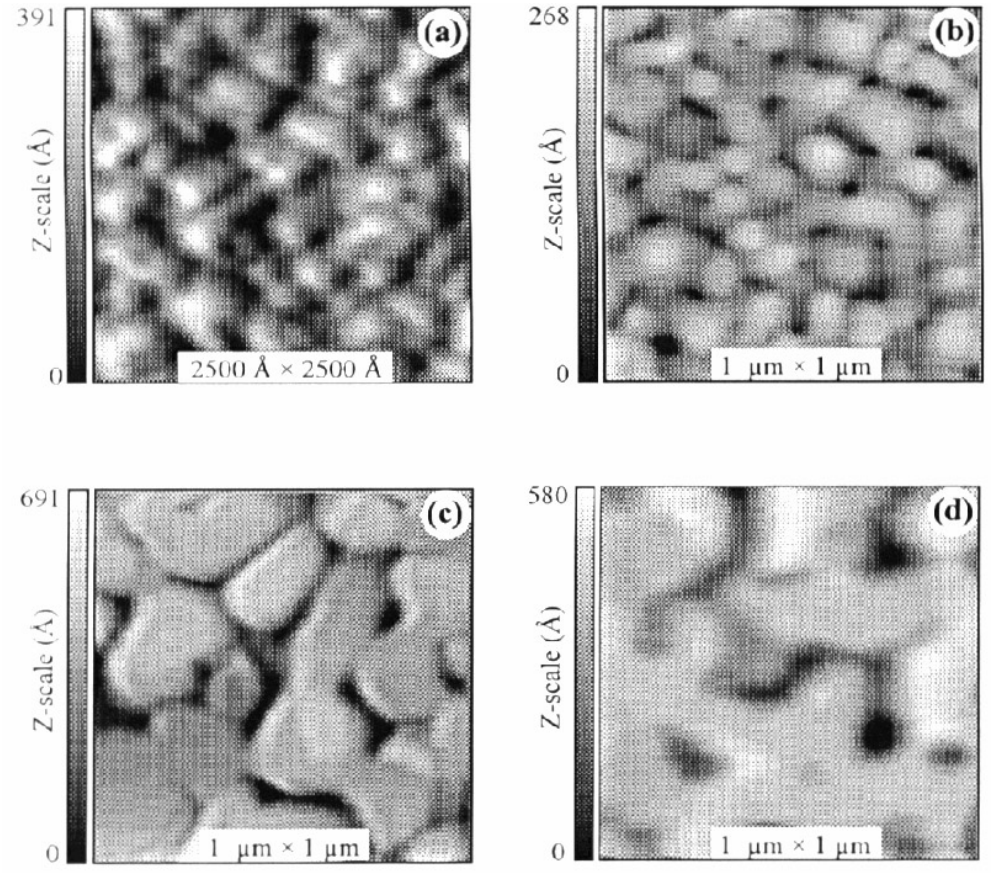

Figure 1. AFM topography of gold films evaporation deposited on mica at four growth temperatures: (a) RT, (b) 150 °C, (c) 300 °C, and (d) 440 °C. The nominal film thickness and the deposition rate used were 1200 Å and ∼1.0 Å s^{-1}, respectively.

Strong dependence of the surface morphology on the growth temperature can be readily identified. When deposited at room temperature (figure 1(a)), rounded mound features dominate the film surface. At a higher growth temperature, such as 150 °C (figure 1(b)), the topographic features of the gold film deposited differ substantially from that deposited at room temperature (figure 1(a)). This higher-temperature preparation is now composed of islands, in the main with flat tops, more or less parallel to the general film surface (figure 1(b)). For the higher-growth-temperature regimes used, such as 300 and 440 °C, the AFM topographic images displayed in figure 1(c) (300 °C) and figure 1(d) (440 °C) show that the surfaces of these two films are now composed of well-oriented and inter-connected structures containing irregular short channels or grooves (figure 1(c) and (d)). At these growth temperatures, gold atoms deposited on the substrate surface (hereafter, the substrate surface referred to in the text refers to both the bare and gold-coated surfaces, where appropriate, when argument is made) have sufficient thermal energy to diffuse over relatively long distances on the surface forming more continuous films containing large, flat, and inter-connected plateaux extending over relatively large areas, separated by channels and voids. In addition to the development of the surface topography with increasing temperature,

it is also obvious that the lateral size of the observed features is increased as well when the growth temperature increases. The origin of these phenomena can be attributed to the exponential dependence of diffusion processes on the actual growth temperature at the substrate surface during deposition. Therefore, as suggested, both adatoms and the surface atoms siting in higher-energy sites are able to travel longer distances at a higher temperature (e.g. $\geqslant 150\,^{\circ}$C), compared to that when at room temperature, before being trapped at equilibrium sites with minimum energy. Such processes will continue during film growth and are enhanced significantly leading to the formation of surfaces with increasing feature dimensions when the growth temperature is further increased. Concerning the *in situ* electron microscope study of gold film formation processes at different temperatures (see e.g. [24]), the joining together of the gold islands to form larger crystallites leading to the formation of a continuous film was found to occur in a manner similar to that of two liquid drops coalescing on a surface. However, the main transport mechanism responsible for this so-called liquid-like behaviour of coalescence has also been attributed to the surface diffusion processes, while the driving force for these processes is the resultant reduction in surface energy. In this regard, there is no difference between these and the arguments made in the text based on the surface diffusion mechanism in the latter case.

The topographical changes observed in the gold film surfaces associated with changes in the nominal thickness are shown in figure 2, together with the image given in figure 1(c). These three films (sample set B) were deposited at 300 °C with three different thicknesses ($H = 100$, 400, 1200 Å) at a fixed deposition rate ($\sim$1.0 Å s^{-1}). When the nominal film thickness, $H = 100$ Å (figure 2(a)), the film consists of well-isolated islands with particular geometries, i.e. the islands appear as regular hexagons (A), asymmetric hexagons (B) and parallelograms (C), as indicated in figure 2(a). Such geometrical crystallite features indicate a Au(111) orientation parallel to the substrate plane and are related to the symmetry of the Au(111) surface itself and the relative in-plane orientations of the neighbouring nucleation sites which coalesce to form the crystallites concerned [25]. No supporting diffraction measurement has been performed here to indicate the extent and nature of this orientation. However, the atomically resolved AFM images obtained from a few such crystallites selected have confirmed the Au(111) orientation. Passing beyond a 100 Å thickness, the well-oriented crystallites grow continuously and coalesce at higher metal coverage to form an inter-connected structure now containing irregular long channels (figure 2(b), $H = 400$ Å) and short channels or grooves (see figure 1(c), $H = 1200$ Å). Both the long and short channels have similar widths, typically $\sim$300–400 Å. At this point (figure 2(b)), the film has coalesced sufficiently to form continuous films also containing large, flat, and inter-connected plateaux over relatively large areas, separated by long channels. Obviously, while retaining the development of plateaux, further deposition of gold causes the channels to be infilled so that the short channels are formed with reduced apparent depth to thickness ratio (e.g. see figure 1(c)) with respect to that of the film containing long channels (figure 1(b)). The transition from island to channel morphology with increase in film thickness was found to occur only at the higher growth temperatures, i.e. $\geqslant 300\,^{\circ}$C as manifest for the given deposition rate ($R \sim 1.0$ Å s^{-1}). This arises because, at high temperature, the significantly increased surface diffusion distance of atoms then allows the gold atoms condensed initially to nucleate and bind with adjacent islands spaced further apart resulting in the formation of larger islands before these themselves begin to touch and coalesce into each other. As long as the larger islands grow to inter-connect, channels are formed.

The AFM topography of the gold films (sample set C) deposited at four different deposition rates with a fixed nominal thickness (400 Å) and a given deposition temperature (440 °C) is shown in figure 3. The evolutions of the surface morphology with deposition

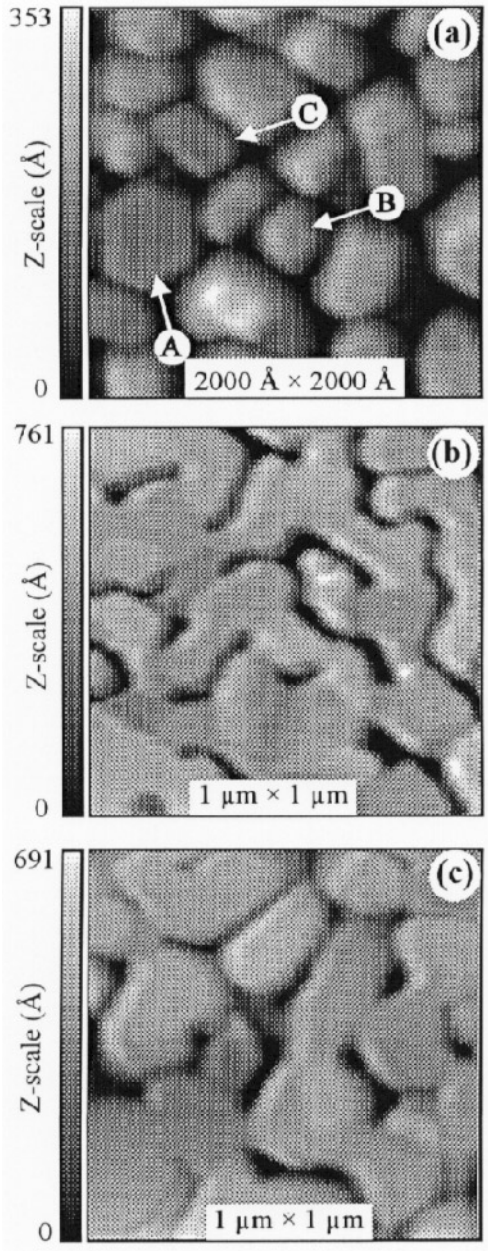

Figure 2. AFM topography of gold films deposited on mica substrates at 300 °C with three different nominal film thicknesses: (a)100 Å, (b) 400 Å, and (c) 1200 Å. The deposition rate used was ∼1.0 Å s^{-1}.

rate, from isolated island to long channel, then to short channel, were also observed here at the given temperature. Obviously, in the lower-deposition-rate range, e.g. < 1.0 Å s^{-1}, the adatoms probably have sufficient time to settle down into equilibrium sites via thermally enhanced surface diffusion processes, before other incoming atoms impact on the surface, so as to form isolated islands (figure 3(a) and (b)). In the higher-deposition-rate range,

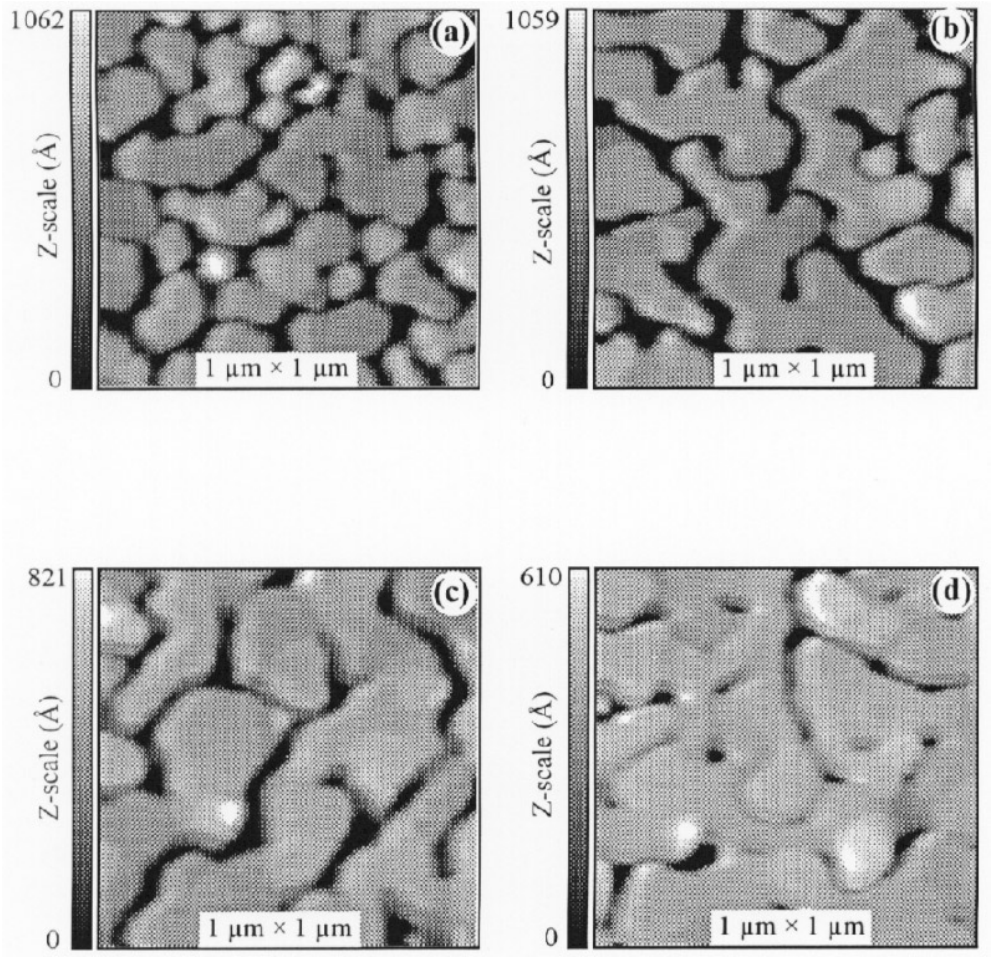

Figure 3. AFM topography of gold films deposited on mica at 440 °C with four different deposition rates: (a) ∼0.26 Å s^{-1}, (b) ∼0.78 Å s^{-1}, (c) ∼2.3 Å s^{-1}, and (d) ∼6.0 Å s^{-1}. The nominal film thickness was 400 Å.

however, non-equilibrium secondary nucleation effects are apparently responsible for the formation of long and short channels because the 'extra' adatoms can result then in these isolated islands becoming inter-connected (figure 3(c)) or these long channels being filled (figure 3(d)) when these atoms settle in sites located within the valleys or the long channels, respectively.

3.2. The self-affine fractal properties

As has been described above, the morphology of these gold film surfaces differs significantly as the preparation conditions used are changed. Typical line-profiles of these features can be seen in figure 4; these were taken from the AFM images shown in figure 1, corresponding to sample set A (H = 1200 Å, R = ∼1.0 Å s^{-1}, T = RT, 150, 300, and 440 °C). The changes in the morphology of the features with growth temperature are obvious. It is worth pointing out that each line-profile given in figure 4 just shows a contour typical of the surface

features at the particular locations in a particular image. The value of P–P height along each line given in figure 4 does not supply any direct information about the surface roughness, because the actual roughness of a surface, as shown in figure 5(a), is characterized by average of the surface feature heights measured at each pixel in a given imaging area or the average of these data obtained from several different areas on the same sample surface. Therefore, the change in P–P height observed in figure 4 with deposition temperature has no direct relation to the roughness change found in figure 5(a) for the corresponding samples.

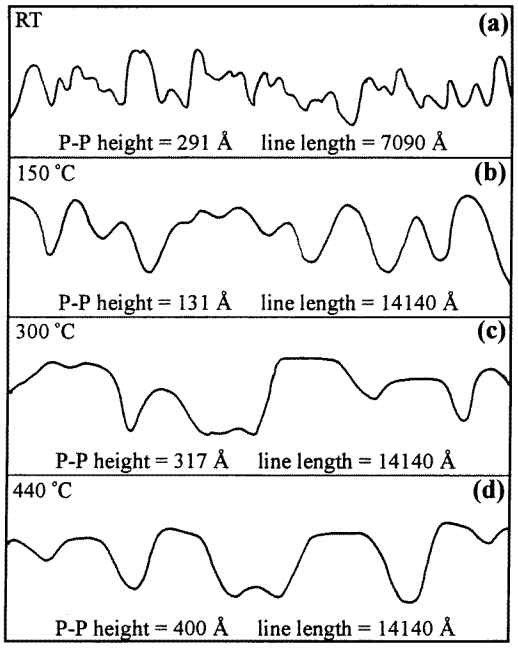

Figure 4. Typical line-profiles taken from the AFM images shown in figure 1, which were acquired from the gold film surfaces deposited at four growth temperatures with a film thickness of 1200 Å using a fixed deposition rate (∼1.0 Å s^{-1}): (a) RT; (b) 150 °C; (c) 300 °C; (d) 440 °C.

Figure 5 shows typical plots of $W_h(L)$ against L and the log–log plots obtained from the AFM images of the gold film surfaces of sample set A using the method described. As can be seen in figure 5(a), the value of the RMS roughness, $W_h(L)$, depends strongly on the lateral scale, L, of the AFM image. Thus $W_h(L)$ increases with L to approach the asymptotic value, W_0, for each individual plot. From the data associated with figure 5, the fractal dimension or roughness exponent, α, for each sample can be obtained by the 'least-squares' simulation of the positive-gradient linear region in the log–log plots using a standard software package. The resultant values of α and the related lateral and height correlation lengths (L_0 and W_0) obtained are given in table 1. The values of the corresponding parameters obtained for the surfaces of sample sets B and C, deposited either with different film thicknesses or at different metal deposition rates respectively, are also listed in table 1. In consequence, the surfaces of gold films evaporation deposited on the mica substrates under the conditions selected in this study can be considered as self-affine fractal in nature, as expected [11, 26, 27]. Clearly, in addition to film thickness, growth

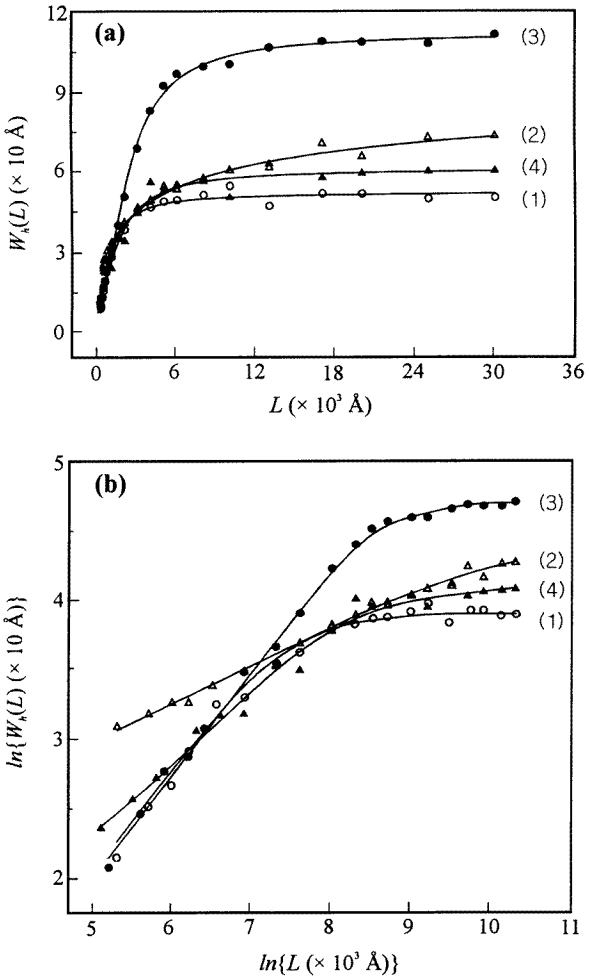

Figure 5. (a) Plots of the average RMS roughness, $W_h(L)$, against the lateral scanning scale, L, and (b) the corresponding $\ln\{W_h(L)\} \sim \ln(L)$ plots. The data shown here were obtained for the gold films as used in figure 1, which were deposited at four growth temperatures using a fixed deposition rate (∼1.0 Å s^{-1}) with a film thickness of 1200 Å: (1) RT; (2) 150 °C; (3) 300 °C; (4) 440 °C.

temperature and deposition rate have in detail a significant effect on the fractal growth behaviour of the surface.

It has been shown [9, 22] for a growing surface, such as a vapour-deposited gold film, that the growth of the surface also correlates with the film thickness (or time) along the growth direction parallel to the surface normal. Moreover, large-scale computer simulation also indicates for film thicknesses larger than a characteristic value, H_c, that the growing surface reaches a steady state [28]. The actual value of H_c depends, therefore, as modelled and as expected, on the detailed deposition conditions under which the rough surface is grown. This is precisely the behaviour observed for the surfaces of sample set B, as shown in table 1, where the scaling parameters (W_0 and α) correlate directly with the thickness of the films deposited at 300 °C. These scaling parameters increase initially with increasing

Table 1. The values of the scaling parameters obtained on the gold film surfaces evaporation-deposited on mica substrates under the different conditions specified.

Group A	T (°C)	RT	150	300	440
$H = 1200$ Å	W_0 (Å)	53	75	108	60
$R \sim 1.0$ Å s^{-1}	L_0 (Å)	1800	30 000	6000	5000
	α	0.74 ± 0.07	0.24 ± 0.01	0.70 ± 0.02	0.57 ± 0.08
Group B	H (Å)	100	400	1200	
$T = 300$ °C	W_0 (Å)	60	113	110	
$R \sim 1.0$ Å s^{-1}	L_0 (Å)	2700	3000	6000	
	α	0.30 ± 0.04	0.75 ± 0.04	0.70 ± 0.02	
Group C	R (Å s^{-1})	∼0.26	∼0.78	∼2.3	∼6.0
$T = 440$ °C	W_0 (Å)	140	154	142	1220
$H = 400$ Å	L_0 (Å)	2840	3460	2040	14 760
	α	0.69 ± 0.03	1.19 ± 0.07	1.45 ± 0.10	0.48 ± 0.03

thickness and then stabilize around constant levels when the film thicknesses, $H \geqslant 400$ Å. Now, for a fixed set of deposition conditions and above a certain thickness, since the nature of the surface of the deposited material does not change further with increasing thickness, both the value of W_0 and α should remain invariant. Despite the fact that it is impossible to estimate accurately the value of the critical thickness, H_c, from the data given in table 1, H_c appears to be around 400 Å, consistent with the value (∼500 Å) reported elsewhere [21] observed for gold surfaces vapour-deposited on smooth glass substrates near room temperature when using a high deposition rate (300 Å s^{-1}). In this regard, for a film thickness $> H_c$, i.e. when the surface of the deposited metal has reached steady state, the roughness exponent, α, as given in table 1, becomes the fundamental parameter for describing the roughness of a self-affine fractal surface grown under a given set of conditions [28]. It is also evident from the data shown in table 1 that, compared to the height correlation length (W_0), the lateral correlation length, L_0, increases with film thickness in the range investigated in this study and no saturation is observed. This differing and thickness-dependent behaviour of the lateral and height correlation lengths indicate an anisotropic evolution of a self-affine fractal surface as defined.

For a given film thickness, however, no direct correlation of surface roughness either with deposition temperature or deposition rate is observed. The scattered distribution of the data for sample sets A and C, given in table 1, simply characterizes each individual rough surface produced from the competition between the self-shadowing and the thermal-enhanced surface diffusion processes, the relevant physical processes operating during film growth.

From the data given in table 1, the values of the roughness exponent, α, measured on most of the sample surfaces concerned in the study made here are in the range 0.24–0.75. Therefore, the results obtained are well consistent with those reported elsewhere using STM data, for gold film surfaces vapour-deposited on glass substrates near room temperature with either high or low deposition rates, e.g. $\alpha = 0.34$ [21], 0.35 ($L >$ the lateral grain size, d_s), and 0.89 ($L < d_s$) [22], as well as comparable with $\alpha = 0.68$–0.82 [15] and 0.5 [29] obtained for vapour-deposited silver film surfaces on mica and glass, respectively, near room temperature. The values of the roughness exponent, α, obtained in the present study also compare well with the exponents 0.67 and 0.35, expected for island-type growth processes which do, or do not, allow for a limited surface mobility of the atoms after striking the

surface [30–32]. This implies that the surfaces of most gold films evaporation-deposited on the mica substrates studied here can be considered as self-affine fractals with the island-type (3D) growth process favoured.

Table 2. The resistance and gold coverage of the gold films deposited under different conditions.

Group A	Growth temperature, T (°C)	RT	150	300	440
$H = 1200$ Å	Coverage	—	0.98	0.93	0.90
$R \sim 1.0$ Å s^{-1}	Resistance (Ω)	2.27	1.17	3.20	0.98
Group B	Film thickness, H (Å)	100	400	1200	
$T = 300$ °C	Coverage	0.79	0.92	0.93	
$R \sim 1.0$ Å s^{-1}	Resistance (Ω)	[a]	25.6	3.20	
Group C	Deposition rate, R (Å s^{-1})	~ 0.26	~ 0.78	~ 2.3	~ 6.0
$T = 440$ °C	Coverage	0.82	0.80	0.91	0.98
$H = 400$ Å	Resistance (Ω)	[a]	[a]	46.2	5.1

[a] > 20 MΩ.

In addition to those data for α discussed above, two cases are identified in which the measured values of α, $\alpha = 1.19$ and 1.45 (the data for sample set C, as given in table 1) are much higher than the others given in table 1 and those referred to above. These high values of α observed in the present study reflect the actual surface topography produced under the growth conditions given, and are borne out by the data on gold coverage and resistance of the two concerned films given in table 2. Here, the resistances given in table 2 were measured for the samples in a 1 cm $\times$ 1 cm lateral scale using a two-probe method. The gold coverage was estimated from the AFM images based on the assumption that the dark regions (i.e. valleys, channels, and holes) seen in the AFM images are related to the areas with zero or near-zero metal coverage and the bright regions (i.e. rounded mounds, islands, and plateaux separated by the channels) represent areas with full coverage. The latter was calculated, therefore, as the fraction of the observed surface covered with the deposited gold with respect to the total surface investigated. Clearly, the topography of these two surfaces is very different from that of the others seen in the related AFM topographical images shown in figures 1–3. The surfaces concerned are composed either of deep valley-isolated, flat-topped large islands evolving towards and near the percolation point [33] (the transition from non-conducting to conducting electrical behaviour) via a coalescence process (figure 3(b), $R \sim 0.78$ Å s^{-1}, gold coverage $\sim$0.8) or coalescence-produced large plateaux well separated by long channels, just at or above the percolation point (figure 3(c), $R \sim 2.3$ Å s^{-1}, gold coverage $\sim$0.91). Obviously, the much more significant thermal-enhanced surface diffusion and reorganization processes of the gold atoms at these growth stages under the relatively high-temperature and intermediate-deposition-rate conditions are responsible for the remarkable lateral development of the deposited film resulting in the formation of self-affine fractal surfaces with high roughness exponents. In other words, the high value of the roughness exponent, α, observed here may indicate a dominant quasi-2D island growth process (the lateral growth of islands greatly exceeding the growth along the vertical direction, compared to the 3D island growth mode referred to above) for gold on mica in this particular case. In fact, the measured values of α ($\alpha = 1.19$ and 1.45) in the present study are consistent with the value of 1.5 predicted from theoretical analysis based on diffusion-dominated growth models of the deposited surfaces [31, 34, 35]. The situation with a high roughness exponent, e.g. $\alpha > 1$, is related obviously to the existence of the

deep valleys and/or the long channels which produce large local near-vertical fluctuations in the associated film surfaces. Here, the long-channel description refers to the extended surface 'troughs' which evolve from the intersecting growth of the deep valleys. In this regard, these two particular gold film surfaces, produced under the conditions selected in the present study, are showing arguably the typical growth models having a high roughness exponent, α, consistent with theoretical prediction. A similar suggestion has also been made elsewhere in the interpretation of the relatively high roughness exponent, α ($\alpha < 1$ in this latter case), of vapour-deposited Au–glass [22] and Ag–mica films [15] near room temperature.

4. Conclusions

A systematic AFM study of gold films deposited on mica substrates under a group of selected conditions reveals and characterizes the evolution of the surface morphology of the films as a function of growth temperature, film thickness, and deposition rate. For the range of thicknesses, deposition rates, and growth temperatures concerned, it is clear that a variety of surface structures, mainly in the form of rounded mounds, islands, and long-channel and short-channel-plateauxed topographical features were formed under the conditions detailed. Moreover, scaling theory, combined with the advent of AFM offering the ready acquisition of 3D surface topographical data, has been used successfully to describe the growth behaviour of the rough surfaces of these gold films prepared as described. Accordingly, the surfaces of the gold films studied here can be considered as self-affine fractals generated either via an island-type (3D) growth process favoured in the majority of cases, with roughness exponent, α, in the range 0.24–0.75, or via a quasi-2D island growth in a minority of cases, with $\alpha = 1.19$ or 1.45. In the latter case, however, the two gold film surfaces grown under the particular conditions used in the present study probably reflect the typical growth models evolving a high roughness exponent, well consistent with theoretical prediction. In consequence, the detailed growth behaviour of the gold film surfaces, i.e. the values of the roughness exponent, α, for each individual surface prepared depends, as is demonstrated, on the actual deposition conditions used.

Acknowledgments

The authors thank the IRCSS at the University of Liverpool and the Chinese Academic Foundation Committee for their support. Thanks are also due to Dr C A Anderson for his help in using the evaporation equipment.

References

[1] Chidsey C E D, Loiacono D N, Sleator T and Nakahara S 1988 *Surf. Sci.* **200** 45
[2] Putnam A, Blackford B L, Jericho M H and Watanabe M O 1989 *Surf. Sci.* **217** 276
[3] DeRose J A, Thundat T, Nagahara L A and Lindsay S M 1991 *Surf. Sci.* **265** 102
[4] Watanabe M O, Kuroda T, Tanaka K and Sakai A 1991 *J. Vac. Sci. Technol.* B **9** 924
[5] Koch R, Winau D, Fuhrmann A and Rieder K H 1992 *Vacuum* **43** 521
[6] Hegner M, Wagner P and Semenza G 1993 *Surf. Sci.* **291** 39
[7] Zheng X Y, Ding Y, Bottomley L A, Allison D P and Warmack R J 1995 *J. Vac. Sci. Technol.* B **13** 1320
[8] Messier R and Yehoda J E 1986 *J. Appl. Phys.* **58** 3739
[9] Vicsek T 1989 *Fractal Growth Phenomena* (Singapore: World Scientific)
[10] Family F and Vicsek T (eds) 1991 *Dynamics of Fractal Surfaces* (Singapore: World Scientific)
[11] Meakin P, Ramanlal P, Sander L M and Ball R C 1986 *Phys. Rev.* A **34** 5091

[12] Krug J and Meakin P 1991 *Phys. Rev.* A **43** 900
[13] Pfeifer P, Yu Y J, Cole M W and Krim J 1989 *Phys. Rev. Lett.* **62** 1997
[14] Eklund E A, Bruinsma R, Rudnick J and Williams R S 1991 *Phys. Rev. Lett.* **67** 1759
[15] Rao M V H, Mathur B K and Chopra K L 1994 *Appl. Phys. Lett.* **65** 124
[16] Eklund E A, Snyder E J and Williams R S 1993 *Surf. Sci.* **285** 157
[17] Miller S and Reifenberger R 1992 *J. Vac. Sci. Technol.* B **10** 1203
[18] Gomez-Rodriguez J M, Baro A M, Vazuiez L, Salvarezza R C, Vara J M and Arvia A J 1992 *J. Phys. Chem.* **96** 347
[19] Mitchell M W and Bonnell D A 1990 *J. Mater. Res.* **5** 2244
[20] Krim J, Heyvaert I, Haesendonck C V and Bruynseraede Y 1993 *Phys. Rev. Lett.* **70** 57
[21] Herrasti P, Ocón P, Vázquez L, Salvarezza R C, Vara J M and Arvia A J 1992 *Phys. Rev.* A **45** 7440
[22] Salvarezza R C, Vázquez L, Herrasti P, Ocón P, Vara J M and Arvia A J 1992 *Europhys. Lett.* **20** 727
[23] Vázquez L, Salvarezza R C, Herrasti P, Ocón P, Vara J M and Arvia A J 1996 *Surf. Sci.* **345** 17
[24] Pashley D W, Stowell M J, Jacobs M H and Law T J 1964 *Phil. Mag.* **10** 127
[25] Allpress J G and Sanders J V 1967 *Surf. Sci.* **7** 1
[26] Meakin P and Krug J 1990 *Europhys. Lett.* **11** 7
[27] Kim J and Kosterlitz J 1989 *Phys. Rev. Lett.* **62** 2289
[28] Family F 1990 *Physica* A **168** 561
[29] Chiarello R, Panella V, Krim J and Thompson C 1991 *Phys. Rev. Lett.* **67** 3408
[30] Kardar M, Parisi G and Zhang Y 1986 *Phys. Rev. Lett.* **56** 889
[31] Wolf D E and Villain J 1990 *Europhys. Lett.* **13** 389
[32] Lai Z W and Sarma S D 1991 *Phys. Rev. Lett.* **66** 2348
[33] Meakin P 1990 *Prog. Solid State Chem.* **20** 135
[34] Sarma S D and Tamborenea P 1991 *Phys. Rev. Lett.* **66** 325
[35] Golubovic L and Bruinsma R 1991 *Phys. Rev. Lett.* **66** 321